USE OF A FUNDAMENTALLY BASED LEAD-ACID BATTERY MODEL IN HYBRID VEHICLE SIMULATIONS

J. N. Harb
Department of Chemical Engineering
Brigham Young University
Provo, Utah 84602-4101

V. H. Johnson and D. Rausen
National Renewable Energy Laboratory
1617 Cole Blvd
Golden, CO 80401

presented at
Annual Electrochemical Society Conference
Seattle, Washington
Spring 1999

ABSTRACT

The purpose of the present study was to combine a detailed fundamental model of a lead-acid battery with the ADVISOR vehicle simulation package developed by the U.S. Department of Energy's National Renewable Energy Laboratory (NREL). Use of fundamentally based models has the potential to significantly increase the predictive capability, flexibility and effectiveness of vehicle simulators as a design tool. Key issues related to integration of such a model are identified and discussed. The model used in the present study is then described and evaluated. Finally, the integrated model is used to simulate the performance of a series-hybrid vehicle through 12 successive FUDS cycles. Successful completion of the vehicle simulations demonstrates the feasibility of using a fundamentally based battery model. The additional information available from such a model is illustrated by the ability of the model to predict a change in the local utilization of the negative electrode as a result of cycling.

INTRODUCTION

Vehicle simulation programs make it possible to investigate and optimize vehicle components and control strategies based on their impact on the entire system performance as predicted by the simulator. In order to make such predictions, the vehicle simulator must include models of all key vehicle components. Such models are often empirical, consisting of look-up tables or correlations of performance data. While these empirical models are ideal for some vehicle components, they can severely limit the predictive capability of the simulator. Replacement of the empirical models with fundamentally based mathematical models has the potential to significantly increase the predictive capability, flexibility and effectiveness of vehicle simulators as a design tool. This paper examines the integration of a fundamental lead-acid battery model with the Matlab-based vehicle simulation program, ADVISOR (1). Of particular interest was the use of the fundamental model for hybrid vehicle simulations. A lead-acid battery was the natural choice for this initial study because of the wealth of literature available on this

system and the fact that much of the initial hybrid vehicle development has been performed with this battery chemistry. The paper begins with a brief review of lead-acid battery models. Issues related to the integration of such a model with ADVISOR are then identified and discussed. This discussion is followed by a description of the battery model used in the present study. Finally, results from the battery model and from the integrated battery model are presented and evaluated.

BATTERY REVIEW

Several different types of battery models of varying complexity and accuracy have been developed. Models developed for use with vehicle simulation packages have typically consisted of look-up tables, equivalent circuits, and/or empirical relationships (2-5). Some aspects of the fundamental behavior have been added into these simple models (6,7). One of the most sophisticated models used for vehicle simulations was reported by Hubbard and Youcef-Toumi (8). These authors adapted a model developed by Ekdunge (7) that was based on the physical and chemical processes that occur in the battery during discharge. Although a considerable step forward, this model was still much less sophisticated than the state-of-the-art battery models found in the literature. For example, the Ekdunge model assumed constant properties across the thickness of the electrode and was not developed to describe behavior during charging.

A number of detailed fundamental models of lead-acid batteries have been reported in the literature (e.g., 9-18), and no attempt has been made to provide an exhaustive review. These models are typically one-dimensional, and include a detailed description of the physical and chemical processes that take place in the battery. It is the description of the key processes that makes this type of battery model useful as a tool for design and optimization. Efforts in recent years have focused on modeling the behavior of recombinant cells which have been increasingly important in commercial applications (16-18). The purpose of the present study was to advance the art of vehicle simulation by combining a detailed fundamental model of a lead-acid battery with the ADVISOR vehicle simulation package.

INTEGRATION OF FUNDAMENTAL MODEL WITH VEHICLE SIMULATOR

Several issues must be addressed in order to integrate a fundamentally based battery model with a vehicle simulation package such as ADVISOR. The modifications to the model that are required to address these issues cover a wide range of complexity and difficulty. Although the issues are discussed in terms of the specific model and vehicle simulation package used in this study, the same issues are relevant to any similar type of combined application.

First, there are often differences between the type of information requested by the vehicle simulator and the typical inputs and outputs used in a fundamental model. For example, current is the natural boundary condition for a fundamental one-dimensional model, and simulations with nearly all such models have been performed at constant current. In contrast, the ADVISOR simulation package required power from the battery pack rather than current. This issue was resolved by adding an external iteration loop that

changed the current until the power was at the specified level at the end of each time step. No attempt was made to match the average power over the time interval since ADVISOR uses a small constant time step of one second. Thus, the error involved in the end of step approximation was not significant.

A second issue that had to be addressed was that of current and voltage limits. Although a power request is made to the battery model, that request must be met within practical constraints. For example, there are practical limits on the current and voltage acceptable for use with the electric motor. If the battery is not capable of supplying the requested power within the specified constraints, then the model must adapt to supply the maximum power possible without violation of the constraints. For example, during discharge this would typically be the power at the lower voltage limit. This adjustment must be made automatically and the detailed model equations must be solved at the limiting conditions to provide the desired output.

Another issue of importance was that the fundamental battery model needed to respond to rapidly changing power requests that switched from one charge or discharge rate to another, or even back and forth from charge to discharge. These frequent changes were needed to satisfy the power demands of, for example, the Federal Urban Driving Schedule (FUDS) (see Fig. 1). Such a cycle is very different from the typical constant current execution mode for this type of battery model. Careful, automated re-initialization of the model was critical to its functionality.

An issue that was critical to the successful use of a fundamental model with the vehicle simulation package was the robustness of the model. It was critical that the fundamental model converge at every point in the simulation. A variety of techniques were used to enhance the stability and/or efficiency of the model such as limiting how far a variable changed in a given iteration, etc. Such techniques are part of the "art of modeling" and are well known to experienced modelers. However, this particular type of application presented a formidable challenge that is not typically addressed in models of this sophistication. It was entirely possible, and, in fact, probable, that the battery model would be asked to meet a request that was physically impossible. For example, more power could be requested than was possible to deliver under the given conditions. A physically impossible situation corresponds to a situation where there is no solution to the model equations. A fundamental model will fail to converge and frequently "blow up" in response to such a request. This problem was mitigated to some extent by the imposition of judicious voltage limits that kept the battery in the appropriate range of operation. However, there were still times when convergence could not be achieved and it was necessary to devise a way of taking a non-converged simulation and readjusting it until convergence could be achieved.

Another issue related to integration was the large number of parameters required for a fundamental model. Some of these, such as rate parameters, should not vary from one lead-acid system to the next. Others are system specific. As hybrid vehicle simulations require simulation of both discharge and charge, parameters and expressions must be adequate in both directions.

The last issue related to integration that will be mentioned here was the actual interface between the ADVISOR simulation package and the fundamental model which,

in this case, was coded in FORTRAN. Development of the interface was greatly facilitated by the fact that ADVISOR was developed in Matlab/Simulink (19). Matlab has a well-documented standard protocol for interfacing with both C and FORTRAN source codes. FORTRAN was used in the present work in order to take advantage of some existing code for linearization and solution of the equations.

DESCRIPTION OF THE FUNDAMENTAL MODEL

Figure 2 is a schematic diagram that illustrates the key features of the one-dimensional model used in this study. The figure shows a unit cell which extends from the center of one electrode to that of the opposite (facing) electrode. The principal reactions at the positive electrode and negative electrodes were as follows:

$$PbO_{2(s)} + 3H^+ + HSO_4^- + 2e^- \underset{\text{charge}}{\overset{\text{discharge}}{\rightleftarrows}} PbSO_{4(s)} + 2H_2O \quad (1)$$

$$Pb_{(s)} + HSO_4^- \underset{\text{charge}}{\overset{\text{discharge}}{\rightleftarrows}} PbSO_{4(s)} + H^+ + 2e^- \quad (2)$$

During charge, both oxygen evolution at the positive electrode and hydrogen evolution at the negative electrode were included in the model. Oxygen recombination at the negative electrode was also included in an approximate way. No attempt was made to model the pressure build-up or mass transfer of gas in the cell. It was believed that the simulation of multiple charge/discharge cycles and the presence of a pressure relief valve in real systems would make detailed tracking of gas compositions and recombination rates difficult. Also, there is still debate in the literature as to what the controlling mechanisms are. Therefore, the present model simply integrated the amount of oxygen evolved in the positive electrode during the previous time step and allowed a specified fraction of that oxygen to recombine at the negative electrode. The recombination was assumed to occur quickly in the outermost computational cell of the negative electrode (closest to the separator). The amount that recombines is also arbitrarily constrained to change by no more than 10% of the total oxygen evolved during the previous time step.

Because the system consisted of three coexistent phases (gas, liquid, and solid), the convective terms that are important in flooded lead-acid cells were not included. In other words, the liquid did not flow due to squeezing out by the solid phase or due to volume changes in the liquid resulting from the reactions at the two electrodes. It was envisioned, however, that the liquid and gas phases would redistribute due to wicking or capillary forces. Mechanistic modeling of such forces was beyond the scope of the present work and inconsistent with the level of assumptions made elsewhere in the model. Consequently, as a first approximation, it was assumed that capillary forces would lead to a volume ratio of gas to liquid that was approximately constant. The volume fraction of liquid was assumed to be constant across the separator, and was updated after each time step based on an overall acid balance.

The equations below are based on the macroscopic description of porous electrodes and use concentrated solution theory to characterize species transport in the electrolyte (20,21). The reversible lead electrode was used as a reference electrode for the solution potential. Activity coefficients (as a function of acid concentration) were approximated by fitting data (22) to a polynomial expression over the range of concentrations from approximately 0.05M to 8M sulfuric acid. The partial molar volumes of electrolyte species were assumed to be constant. The expressions used to describe the reaction rates accounted for mass transfer limitations due to dissolution of Pb^{+2} (18,23). Finally, the matrix potential (potential of the solid phase) was assumed to be constant over the thickness of each electrode (i.e. in the radial direction). Calculations showed that the matrix potential changed very little relative to the change in the solution potential across the electrode. This assumption allowed elimination of an equation and hence simplified and increased the efficiency of the calculations. A detailed listing of the model equations for the negative electrode only are listed below, in an effort to keep this document as short as possible. A similar set of equations was used for the positive electrode. The equations in the separator were the same as those of Bernardi and Carpenter (17). In addition, an overall volume balance for the electrolyte was used to determine the liquid volume fraction in the separator.

Pb Electrode

Solid material balance:

$$\frac{\partial \varepsilon_s}{\partial t} = \frac{1}{2F}\left| \frac{M_{PbSO_4}}{\rho_{PbSO_4}} - \frac{M_{Pb}}{\rho_{Pb}} \right| j_{Pb} \tag{3}$$

Cell volume balance:

$$\varepsilon_s + \varepsilon_l + \varepsilon_g = \varepsilon_s + (1+\lambda)\varepsilon_l = 1 \tag{4}$$

where λ is the ratio of the gas to liquid volume fractions.

Ohm's Law in the liquid phase:

$$\frac{i}{\kappa^{eff}} = -\frac{\partial \phi_l}{\partial x} + \frac{RT}{F}\left(1-2t_+^o\right)\frac{\partial \ln(c_A f)}{\partial x} \tag{5}$$

Material balance for the acid:

$$\frac{\partial(\varepsilon_l c_A)}{\partial t} = \frac{\partial}{\partial x}\left| D_A^{eff} \frac{\partial c_A}{\partial x} \right| + \frac{1}{2F}\left(1-2t_+^o\right) j_{Pb} + \frac{1}{F}\left(1-t_+^o\right) j_{O_2} + \frac{1}{F}\left(1-t_+^o\right) j_{H_2} \tag{6}$$

where movement of the acid by capillary forces was not accounted for in Eq. 6.

Reaction rate:

$$j_{Pb} = \frac{2Fk_{PbSO_4,Pb}c_{Pb^{2+}}^{sat}a_{\max,Pb}i_{o,Pb}\left|1-\frac{Q}{Q_{\max,Pb}}\right|^{\delta_1}\left(\frac{Q}{Q_{\max,Pb}}\right)^{\delta_1}\left[\exp\left(\frac{(\alpha_{a,Pb}+\alpha_{c,Pb})F}{RT}(\phi_s-\phi_l)\right)-1\right]}{i_{o,Pb}\left(\frac{Q}{Q_{\max,Pb}}\right)^{\delta_1}+2Fk_{PbSO_4,Pb}c_{Pb^{2+}}^{sat}\left(1-\frac{Q}{Q_{\max,Pb}}\right)^{\delta_1}\exp\left(\frac{\alpha_{c,Pb}F}{RT}(\phi_s-\phi_l)\right)} \quad (7)$$

And finally, the current balance:

$$\frac{\partial i}{\partial x} = j_{Pb} + j_{O_2} + j_{H_2} \quad (8)$$

The expression for the reaction rate (eq. 7) is essentially that presented by Newman and Tiedemann (18), except that a typographical error in their paper was corrected. A similar expression was used for the positive electrode. The equilibrium potential between Pb and PbO_2 was determined with use of the expression developed by Bode (22). A correlation for the activity coefficient was obtained by fitting data from Bode (22). Relationships for the effective diffusion coefficient and electrolyte conductivity as a function of composition and temperature were taken from Nguyen et al. (15).

The complete equation set was reduced to two coupled equations that were solved numerically at each time step with use of Newman's BAND subroutine. The total number of nodal points used in the calculation was kept at a minimum, typically 15, in order to reduce the computational time required. Nodal points were located at the center of the control volumes and were non-uniformly spaced in order to increase their effectiveness. The magnitude of the time step was normally determined by the calling routine. However, if the requested time interval was large, it was automatically divided into an equal number of smaller time steps whose size was dependent on the magnitude of the current.

RESULTS

Model Validation

Before integration of the detailed model with the vehicle simulation program, battery simulations were performed in constant current mode and results were compared to discharge data from single cells. The results are shown in Fig. 3 for two different discharge rates. The same set of parameters (see Nguyen et al. (15)) was used for the simulations at both rates. The simulations were performed with the rate expressions that include limitations due to the mass transfer of Pb^{+2} (eq. 7 for the negative electrode and a similar expression for the positive electrode). Because mass transfer of Pb^{+2} is less important during discharge, the expressions of Nguyen et al. and the expressions used in the present study yielded similar results for discharge. Figure 4 provides a comparison of the predictions at the 5C rate with two additional simulations: 1) simulation of discharge at the 5C rate with the parameters of Newman and Tiedemann (18), and 2) simulation of discharge at the 5C rate with the parameters and rate expressions of Bernardi and

Carpenter (17). Note that the rate expressions of Newman and Tiedemann are equivalent during discharge to those used in the present study. Poor agreement was observed between the measured data and the additional predictions. Both sets of parameters used in the additional predictions were developed to simulate charging and are clearly unsuitable for discharge simulations. However, it was expected that either of these sets would yield better results during charging. Comparison with charging data showed that this was not the case and that the parameters of Nguyen et al. led to better agreement between measured and predicted results during both charge and discharge. These results illustrate the difficulty associated with obtaining useful parameters and emphasize the fact that caution must be used when taking data from the literature. A list of the parameters used in the present simulations is provided in Table I. Parameters specific to the design of the prototype hybrid vehicle battery simulated in this study have not been included in the table for proprietary reasons.

As mentioned previously, one of the principal concerns with the integration of a fundamental model with a vehicle simulation program was the robustness of the model. The fundamental model would not be useful if it "crashed" frequently in the middle of vehicle simulations. For this reason, efforts were made to prevent the model from "blowing up" by limiting the amount that a variable could change from iteration to iteration. In situations where convergence could not be reached, the calculation was reinitialized at a lower current density and attempted again. This procedure continued until a satisfactory solution was reached. The impact on the model is illustrated in Fig. 5 which shows a high power discharge that continued until acid depletion was evident in the positive electrode. The specified minimum voltage was reached at a time of 115s, and the power was subsequently reduced gradually to avoid going below the minimum voltage value. The simulation continued until the model failed to converge. The model was able to recognize the problem and respond automatically by lowering the power until an adequate numerical solution was found. The simulations then continued at the lower power until it was necessary to again reduce the rate. The discrete reductions in power led to the step-like behavior apparent towards the end of the simulation. However, the model was able to adjust automatically to a situation where it was physically impossible to deliver the power requested. Such situations are avoided to a large extent by the application of appropriate voltage limits, and the model was able to deal with almost all of them without crashing. In other words, the present model appeared to be sufficiently robust for use with a vehicle simulation package.

Results From the Integrated Model

The fundamental battery model described above was integrated into the vehicle simulation program ADVISOR. The input needed for the fundamental model was placed in Matlab "m" files and was accessible to change by the user during the initiation phase of the ADVISOR simulation. After initiation and before performance of the simulation, the input was "dumped" to the four input files needed by the fundamental model. The first file contained fundamental parameters such as reaction rate constants, partial molar volumes, etc. The second file contained numerical parameters such as the number of nodal points and the spacing of nodes. The third file contained specific information on the battery being simulated including the size, thickness and porosity of electrodes, electrode capacity, the acid concentration, the volume fraction of supporting

Table I. Model Parameters

Symbol	Description	Value [a]
$a_{max,Pb}$	Initial internal surface area for Pb electrode (cm^{-1})	23000.
$a_{max,PbO2}$	Initial internal surface area for PbO_2 electrode (cm^{-1})	230000.
$c_{A,ref}$	Reference acid concentration (mole/cm^3)	0.00494 (17)
f_{O2}	Fraction of oxygen recombined at negative electrode	0.99[b]
$i_{o,H2}$	Exchange current density for H_2 at negative electrode (A/cm^2)	$6.607x10^{-14}$ (24)
$i_{o,O2}$	Exchange current density for O_2 at positive electrode (A/cm^2)	$1.3x10^{-14}$ (18)
$i_{o,Pb,ref}$	Reference exchange current density, Pb electrode at 25°C (A/cm^2)	$4.96x10^{-6}$
$i_{o,PbO2,ref,}$	Reference exchange current density, PbO_2 electrode at 25°C (A/cm^2)	$3.19x10^{-7}$
$k_{PbSO_4,Pb}c^{sat}_{Pb^{2+}}a_{max,Pb}$	Mass transfer parameter, negative electrode (mol/cm^3 s)	$5.75x10^{-4}$ [b]
$k_{PbSO_4,PbO_2}c^{sat}_{Pb^{2+}}a_{max,PbO_2}$	Mass transfer parameter, positive electrode (mol/cm^3 s)	0.023[b]
T	Initial cell temperature (K)	298[b]
t^o_+	Transference number for Hydrogen Ion	0.72
U_{H_2}	Thermodynamic potential for H_2 (V)	0.356(18)
U_{O_2}	Thermodynamic potential for O_2 (V)	1.649(17)
$\bar{V}_A$	Partial Molar Volume of Acid (cm^3/mole)	45.(17)
$\bar{V}_o$	Partial Molar Volume of Water (cm^3/mole)	17.5(17)
α_{a,O_2}	Anodic charge transfer coefficient for O_2	0.657(18)
$\alpha_{a,Pb}$	Anodic charge transfer coefficient for Pb electrode	1.55
α_{a,PbO_2}	Anodic charge transfer coefficient for PbO_2 electrode	1.15
α_{c,H_2}	Cathodic charge transfer coefficient for H_2	0.58(24)
$\alpha_{c,Pb}$	Cathodic charge transfer coefficient for Pb electrode	0.45
α_{c,PbO_2}	Cathodic charge transfer coefficient for PbO_2 electrode	0.85
δ_1	Exponent for area correction, Pb electrode	1.5
δ_2	Exponent for area correction, PbO_2 electrode	1.5
$\varepsilon_{g,sep}$	Fraction of gas in separator	0.10 [b]
$\varepsilon_{s,sep}$	Separator volume fraction	0.08 (17)
γ_1	Exponent for concentration dependence of exchange current density (Pb)	$1.0x10^{-4}$
γ_2	Exponent for concentration dependence of exchange current density (PbO_2)	0.3
λ	Ratio of gas to liquid volume in the electrodes	0.10[b]
ρ_{Pb}	Density of Pb (g/cm^3)	11.34 (17)
ρ_{PbO2}	Density of PbO_2 (g/cm^3)	9.7 (17)
ρ_{PbSO4}	Density of $PbSO_4$ (g/cm^3)	6.3 (17)

[a] Values from Ref. 15 unless otherwise noted.
[b] Assumed

grid, etc. As mentioned above, these parameters have not been listed in the paper for proprietary reasons. The last file contained the specified current and voltage limits. The current limit was typically a function of the electric motor used. The voltage could be limited by the motor specifications or, more commonly, by a range acceptable for battery operation. In the present integration, the fundamental model provided results for a six-cell module. In practice this was done by performing calculations for a single cell and then scaling linearly to the desired size. Cell-to-cell variations were not accounted for. An additional resistance was added to account for terminal losses associated with each cell. The scaling from module to pack was done internally in ADVISOR, and the fundamental model did not account for losses between the 25 modules that made up the battery pack.

Figure 6 provides an example of results obtained with the integrated model for a series-hybrid vehicle performing 12 successive FUDS cycles. The total distance traveled in the simulations was approximately 80 miles. Figure 6a shows power delivered to/from the battery as a function of time. Note that ADVISOR works on a one second cycle so that the power request could be changed as frequently as once per second. Discussion of the control algorithm used in the simulations is beyond the scope of the present paper. Figure 6b shows the state-of-charge of the battery which was based on the rated capacity (16.5 Ahr) and allowed to vary between 0.4 and 0.8 in this particular simulation. The power delivered by the generator is shown in Fig. 6c.

The model was only recently brought to this level of functionality so that the information available has only begun to be explored. For example, Fig. 7 shows the local utilization of the negative electrode at the high and low states of charge for the first and last FUDS cycles in the above simulation. From this figure it is apparent that cycling changed the distribution of charge in the electrode. Such changes will likely affect battery performance over the lifetime of the vehicle. Note that the distance traveled in the simulation was only about 80 miles.

CONCLUSIONS

A fundamentally based lead-acid battery model has been developed and integrated into the vehicle simulation package ADVISOR. A key issue related to model integration was the need to converge the model in response to rapidly changing power requests that may exceed the capability of the batteries. Another important issue was the need for parameters suitable for simulation of both charge and discharge. The integrated model was used successfully to simulate the performance of a series-hybrid vehicle through 12 successive FUDS cycles, corresponding to a total distance of approximately 80 miles. Results from the simulations include the power output from the battery pack, the state-of-charge, and power output from the generator as a function of time. These simulations demonstrate the feasibility of using a fundamentally based battery model for the simulation of hybrid vehicle performance. In addition, this type of model provides details about the battery not previously available. For example, the model was able to predict a change in the local utilization of the negative electrode that occurred as a result of cycling.

ACKNOWLEDGMENTS

Funding for this work by the National Renewable Energy Laboratory (NREL) is gratefully acknowledged.

REFERENCES

1. K. Wipke, et al., North American EV & Infrastructure Conference (1998).
2. B.K. Powell and T.E. Pilutti, *Proceedings of the 33rd IEEE Conference on Decision and Control*, 94-12, p. 2736 (1994).
3. V.P. Roan and A. Raman, *Proceedings of the 28th Intersociety Energy Conversion Engineering Conference*, 93-8, p. 229 (1993).
4. F.E. Wicks and D. Marchionne, *Proceedings of the 27th Intersociety Energy Conversion Engineering Conference*, 92-8, p. 3.151 (1992).
5. K.E. Bailey and B.K. Powell, *Proceedings of the 1995 American Control Conferences*, 95-6, p. 1677 (1995).
6. M.C. Glass, *Proceedings of the 31st Intersociety Energy Conversion Engineering Conference*, 96-8, p. 292 (1996).
7. P. Ekdunge, *J. Power Sources*, **46**, 251 (1993).
8. Hubbard, G.A., Youcef-Toumi, K., *Proceedings of the 1997 American Control Conference*, 97-6, p. 636 (1997).
9. W. Tiedemann and J. Newman, in *Battery Design and Optimization*, Sid Gross, Editor, p.23, The Electrochemical Society Proceedings Series, Pennington, NJ, (1979).
10. W.G. Sunu, in *Electrochemical Cell Design*, R.E. White, Editor, p. 357, Plenum Publishers, New York, NY, (1984).
11. H. Gu, T.V. Nguyen, and R.E. White, *J. Electrochem. Soc.*, **134**, 2953 (1987).
12. D.M. Bernardi, GM Research Publication GMR-6289, Oct 9 (1988).
13. E. C. Dimpault-Darcy, T. V. Nguyen and R. E. White, *J. Electrochem. Soc.*, **135**, 278 (1988).
14. R.M. LaFollette and D.N. Bennion, *J. Electrochem. Soc.*, **137**, 3701 (1990).
15. T.V. Nguyen, R.E. White and H. Gu, *J. Electrochem. Soc.*, **137**, 2998 (1990).
16. T.V. Nguyen and R.E. White, *Electrochim. Acta*, **38**, 935 (1993).
17. D.M. Bernardi and M.K. Carpenter, *J. Electrochem. Soc.*, **142**, 2631 (1996).
18. J. Newman and W. Tiedemann, *J. Electrochem. Soc.*, **144**, 3081 (1997).
19. SIMULINK (Version 2) and MATLAB (Version 5.2), The Math Works, Inc., 1998.
20. J. Newman and W. Tiedemann, *AIChE Journal*, **21**, 25 (1975).
21. J. Newman, *Electrochemical Systems*, 2nd Ed., Prentice-Hall, Princeton, NJ (1991).
22. H. Bode, *Lead Acid Batteries*, Wiley and Sons, New York, NY (1977).
23. J.S. Dunning, D.N. Bennion, and J. Newman, *J. Electrochem. Soc.*, **118**, 1251 (1971).
24. L.T. Lam, J.D. Douglas, R. Pillig and D.A.J Rand, *J. Power Sources*, **48**, 219 (1994).

NOMENCLATURE
(Variables Not Listed in Table I)

Variable	Definition
c_A	Acid Concentration (mole/cm^3)
D_A	Diffusion Coefficient of Acid (cm^2/sec)
f	Mean Molar Activity Coefficient
F	Faraday's Constant (96485 C/eq)
R	Gas Constant (8.314 J/mole/°K)
i	Superficial Current Density in Electrolyte Solution (A/cm^2)
i_o	Exchange Current Density (A/cm^2)
j	Transfer Current (A/cm^3)
M_i	Molecular Weight of Species i (g/mole)
Q	Specific Capacity (C/cm^3)
Q_{max}	Fully Charged Capacity (C/cm^3)
t	Time (sec)
U	Open Circuit Potential (V)
ε	Volume Fraction
ϕ	Potential (V)
κ	Electrolyte Conductivity (S/cm)

Subscripts

g	Gas
l	Liquid
Pb	Negative Electrode
PbO_2	Positive Electrode
ref	Reference
s	Solid

Superscripts

eff	Effective

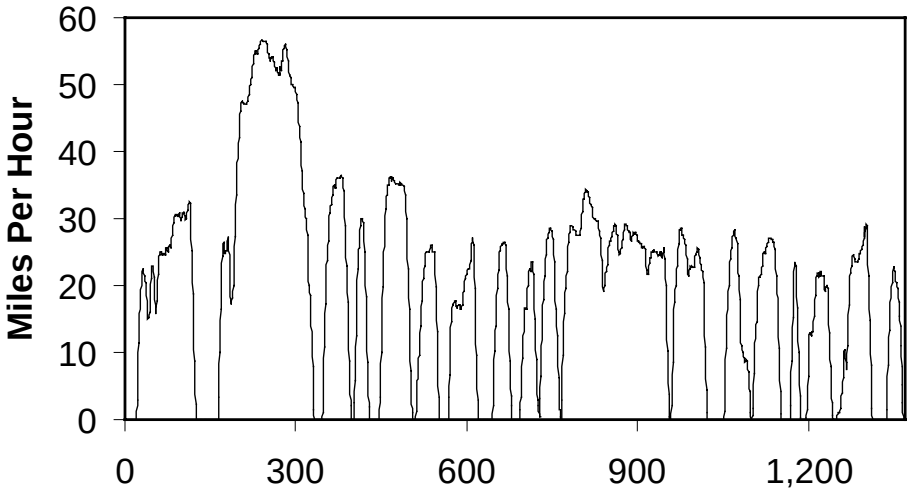

Figure 1. Federal Urban Driving Schedule

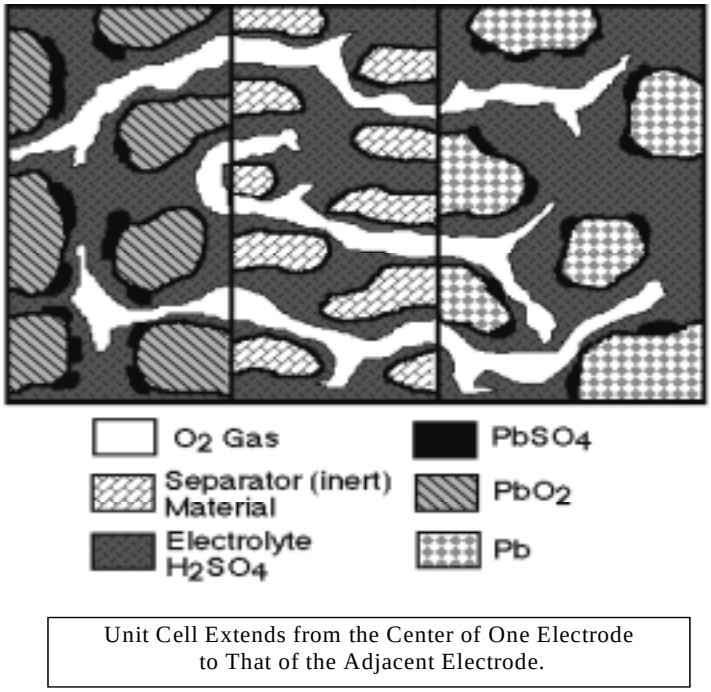

Figure 2. Schematic diagram of lead-acid battery cell

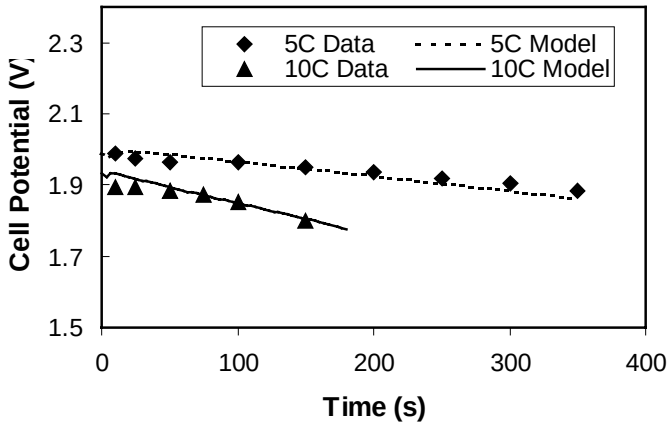

Figure 3. Comparison of battery model predictions with data at two different discharge rates.

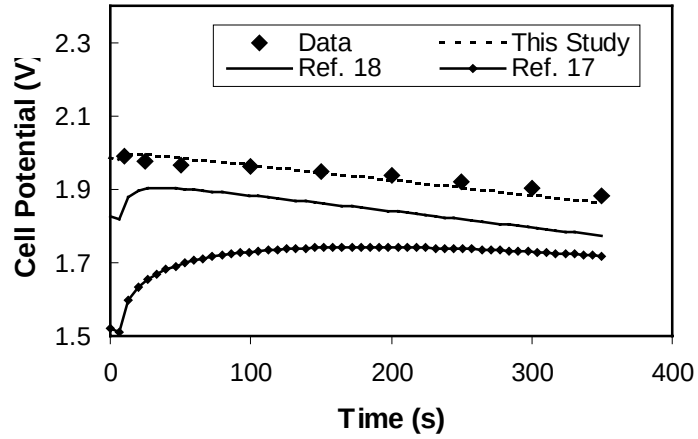

Figure 4. Comparison of predictions with different parameters.

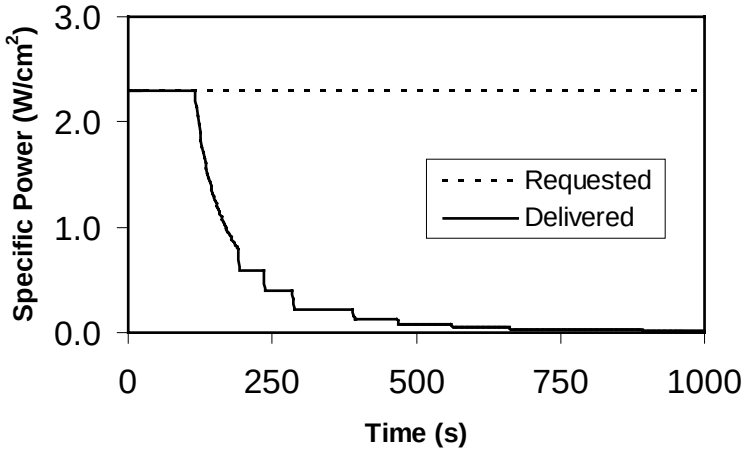

Figure 5. Response of model to constant power request.

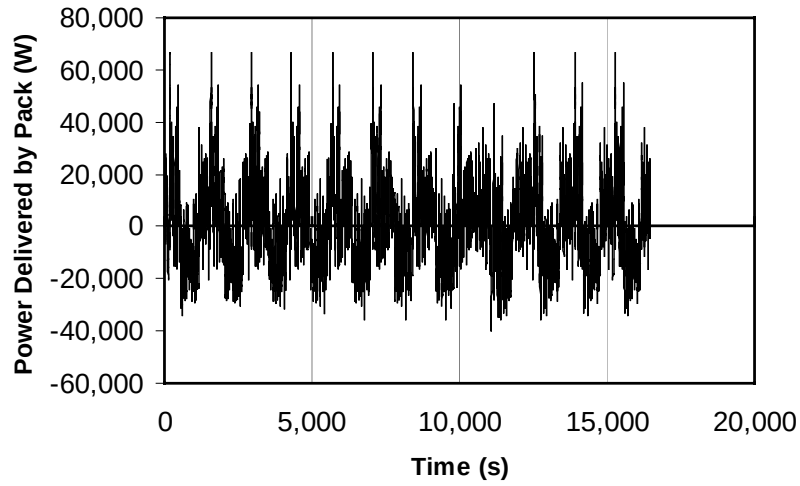

(a)

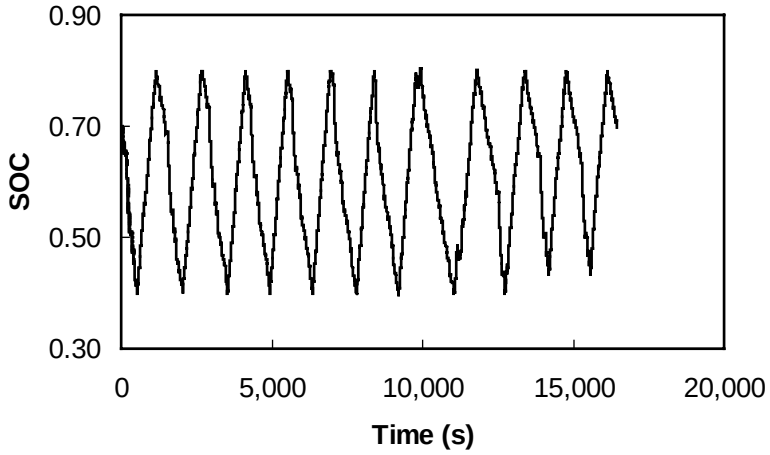

(b)

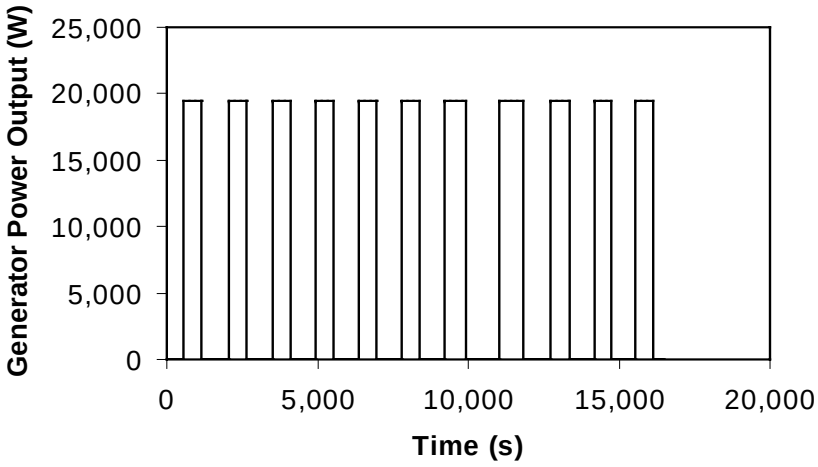

(c)

Figure 6. Simulation results for 12 successive FUDS cycles: a) power delivered/consumed by pack, b) state-of-charge, c) generator output.

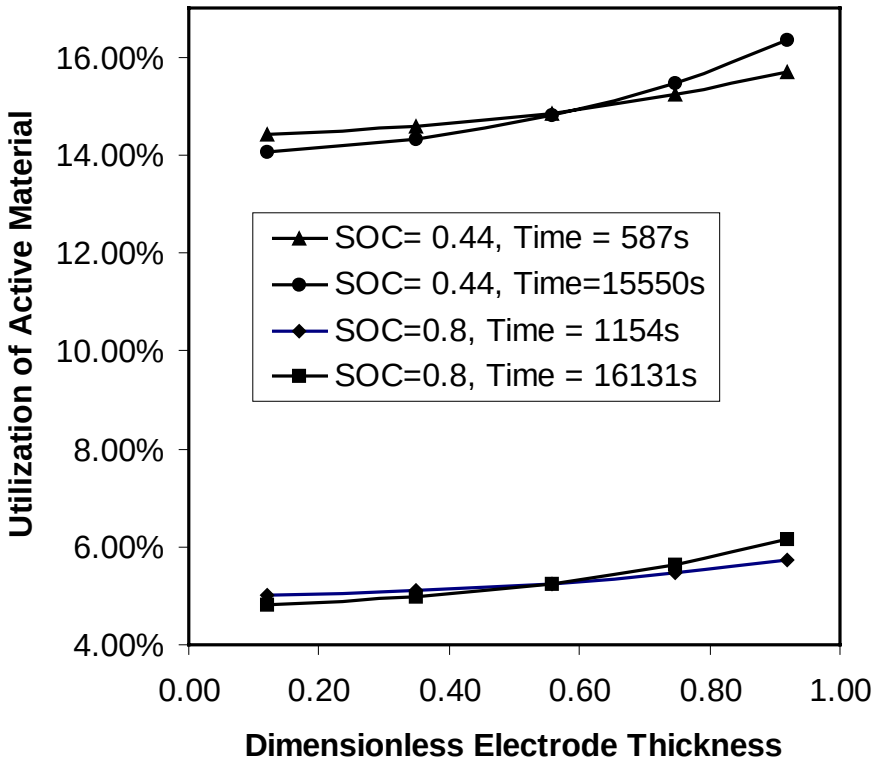

Figure 7. Local electrode utilization as a function of SOC and cycling time.